Journal of Colloid and Interface Science 440 (2015) 140–150

Contents lists available at ScienceDirect

Journal of Colloid and Interface Science

www.elsevier.com/locate/jcis

Experimental investigation of virus and clay particles cotransport in partially saturated columns packed with glass beads

Vasiliki I. Syngouna [a], Constantinos V. Chrysikopoulos [b,*]

[a] Environmental Engineering Laboratory, Civil Engineering Department, University of Patras, Patras 26500, Greece
[b] School of Environmental Engineering, Technical University of Crete, Chania 73100, Greece

ARTICLE INFO

Article history:
Received 23 August 2014
Accepted 26 October 2014
Available online 6 November 2014

Keywords:
Unsaturated porous media
Viruses
Colloids
Cotransport
Attachment efficiency
DLVO
Capillary forces

ABSTRACT

Suspended clay particles in groundwater can play a significant role as carriers of viruses, because, depending on the physicochemical conditions, clay particles may facilitate or hinder the mobility of viruses. This experimental study examines the effects of clay colloids on the transport of viruses in variably saturated porous media. All cotransport experiments were conducted in both saturated and partially saturated columns packed with glass beads, using bacteriophages MS2 and ΦX174 as model viruses, and kaolinite (KGa-1b) and montmorillonite (STx-1b) as model clay colloids. The various experimental collision efficiencies were determined using the classical colloid filtration theory. The experimental data indicated that the mass recovery of viruses and clay colloids decreased as the water saturation decreased. Temporal moments of the various breakthrough concentrations collected, suggested that the presence of clays significantly influenced virus transport and irreversible deposition onto glass beads. The mass recovery of both viruses, based on total effluent virus concentrations, was shown to reduce in the presence of suspended clay particles. Furthermore, the transport of suspended virus and clay-virus particles was retarded, compared to the conservative tracer. Under unsaturated conditions both clay particles facilitated the transport of ΦX174, while hindered the transport of MS2. Moreover, the surface properties of viruses, clays and glass beads were employed for the construction of classical DLVO and capillary potential energy profiles, and the results suggested that capillary forces play a significant role on colloid retention. It was estimated that the capillary potential energy of MS2 is lower than that of ΦX174, and the capillary potential energy of KGa-1b is lower than that of STx-1b, assuming that the protrusion distance through the water film is the same for each pair of particles. Moreover, the capillary potential energy is several orders of magnitude greater than the DLVO potential energy.

1. Introduction

Several theoretical and experimental investigations have shown that suspended mobile colloids can either facilitate or hinder the mobility of various contaminants in water saturated porous and fractured media [1–11]. However, colloid facilitated virus transport in unsaturated porous media is substantially different and more complex than that in saturated porous media. In addition to the retention mechanisms governing colloid and virus transport in saturated porous media (e.g., pore straining and attachment onto solid-water interfaces (SWI)), colloids in unsaturated porous media can be retained at air–water interfaces (AWI), in thin water films (film straining), and air–water–solid (AWS) interfaces [12–26]. Furthermore, in unsaturated porous media, colloids and viruses can also be retained in air–water meniscus–solid (AW_mS) interfaces [27,28]. Note that AW_mS interfaces are essentially areas where significant colloid attachment occurs and water meniscuses diminish to thin water films.

Capillary forces are known to be important for colloid attachment at the AWI as well as for film straining [12,14,25,29,30]. Derjaguin–Landau–Verwey–Overbeek (DLVO) interactions cannot always explain the observed colloid deposition in unsaturated porous media [17,30], especially at the contact line of the AW_mS interface. Colloid retention of the AW_mS interface is explained more convincingly by capillary force interactions [23,24,31]. Despite of these and other related research efforts, the role of capillary forces on colloid retention in unsaturated porous media is not fully understood and deserves more attention.

The objective of this paper was to explore further the specific interactions of simultaneously transported colloids and viruses with the various interfaces (SWI, AWI, and AWS) present in

* Corresponding author.
E-mail address: cvc@enveng.tuc.gr (C.V. Chrysikopoulos).

http://dx.doi.org/10.1016/j.jcis.2014.10.066
0021-9797/

unsaturated porous media. Also, the synergistic effects of suspended clay colloids and water saturation level on the attenuation and transport of viruses in unsaturated porous media is examined. Furthermore, the surface properties of viruses, clays, and glass beads are used to construct classical DLVO and capillary potential energy profiles, which are evaluated.

2. Materials and experimental procedures

2.1. Bacteriophages and assay

The bacteriophage MS2 (F-specific single-stranded RNA phage with effective particle diameter ranging from 24 to 26 nm), and ΦX174 (somatic single-stranded DNA phage with effective particle diameter ranging from 25 to 27 nm) were used as model viruses. Both bacteriophages are infecting *E. coli,* and were assayed by the double-layer overlay method [32], as outlined by Syngouna and Chrysikopoulos [33]. Viruses attached onto clay particles were separated from viruses suspended in the liquid phase by centrifugation at 2000*g* for 30 min [10]. The suspension of unattached viruses in the supernatant was pipetted out, and the concentration of the suspended viruses was determined. The absence of clay colloids in the supernatant was verified by a UV–vis spectrophotometer (UV-1100, Hitachi) at a wavelength of 280 nm. The concentration of attached viruses was determined by subtracting the mass of viruses that remained in suspension from the initial virus concentration in each sample.

2.2. Clays

The clays used in this study were kaolinite (KGa-1b, a well-crystallized kaolin from Washington County, Georgia) and montmorillonite (STx-1b, a Ca-rich montmorillonite, white, from Gonzales County, Texas), purchased from the Clay Minerals Society, Columbia, USA. The < 2 μm colloidal fraction of each clay mineral suspension in sterile ddH_2O was separated by sedimentation and was purified following the procedure described by Rong et al. [34]. The optical density of the clay colloids was analyzed at a wavelength of 280 nm by a UV–vis spectrophotometer, and the corresponding clay concentrations were determined as outlined by Chrysikopoulos and Syngouna [35]. The hydrodynamic diameter of the clay colloids was measured by a zetasizer (Nano ZS90, Malvern Instruments) and was found to be equal to $d_p = 843 \pm 126$ nm for KGa-1b, and $d_p = 1187 \pm 381$ nm for STx-1b [35].

2.3. Porous media

Glass beads were used as the packing material of the columns in order to eliminate possible experimental difficulties associated with real soil, which may provide numerous uncertainties that can complicate considerably the analysis of the experimental data. Following the procedure previously described by Syngouna and Chrysikopoulos [10], the glass beads were purified until the water conductivity, as determined by a conductivity meter, was negligible. The glass beads were dried in an oven at 105 °C, and then stored in screw cap sterile beakers until use in the column experiments.

2.4. Electrokinetic measurements

The Zeta potentials, ζ [V], of the bacteriophages and clays, measured at pH 7 in sterile ddH_2O by the zetasizer (Nano ZS90, Malvern Instruments, Southborough, MA), were $\zeta = -40.4 \pm 3.7$ mV for MS2, $\zeta = -31.8 \pm 1.3$ mV for ΦX174, $\zeta = -26.0 \pm 2.8$ mV for KGa-1b, and $\zeta = -20.5 \pm 0.8$ mV for STx-1b [35]. Furthermore, the zeta potential of glass beads stored in ddH_2O at pH 7 was determined to be $\zeta = -54.6 \pm 2.4$ mV [10]. The zeta potential for the AWIs present in the unsaturated packed columns was obtained from the literature ($\zeta = -65$ mV in ddH_2O solution) [15,36].

2.5. Column experiments

All flow-through experiments were conducted using Plexiglas columns with length 15.2 cm and internal diameter 2.6 cm. The experimental setup is similar to that described in detail by Mitropoulou et al. [37]. Briefly, the column was uniformly wet-packed with glass beads. Several pore volumes of the de-aired sterile ddH_2O were passed through the column from the bottom to avoid the capture of air bubbles. The packed column was vertically attached to a vacuum chamber (Soil Measurement Systems, Tucson, AZ) with a fraction collector inside, which allowed for various levels of water saturation. Due to the relatively small size of the viruses used in this study, gravity effects were assumed to be negligible [38]. The water potential and the uniformity of water in the column were verified with tensiometer readings, which were collected continuously using a CR800 datalogger (Campbell Scientific, Inc., Logan, UT). Liquid samples were collected at regular time intervals from the column effluent in small fractions with an automatic fraction collector.

A fresh column was packed for each experiment. The entire packed column and glassware used for the experiments were sterilized in an autoclave at 121 °C for 20 min. Constant flow of ddH_2O at flow rate of $Q = 1.5$ mL/min in the vertical-down direction was used. The mean pH of the column influent remained constant at 7.0 ± 0.2 for the duration of each experiment. One set of experiments was performed with viruses and clay particles alone in order to determine their individual transport characteristics. Another set of cotransport experiments was performed to investigate the effect of the presence of clay colloids on virus transport. The clay colloidal suspension and the viral suspension were injected simultaneously into the packed column, at the same flow rate, for 3 pore volumes, followed by 3 pore volumes of ddH_2O. All experiments were carried out at room temperature (~25 °C). Chloride, in the form of potassium chloride (KCl), was chosen as the nonreactive tracer. All effluent chloride concentrations were measured using ion chromatography (ICS-1500, Dionex Corp., Sunnyvale, CA).

3. Theoretical considerations

3.1. Moment analysis

The colloid concentration breakthrough data obtained at the end of the packed column ($x = L$) were analyzed by the first normalized temporal moment, M_1 [t] [39]. In this study, four different $M_{1(i)}/M_{1(t)}$ ratios of the first normalized temporal moment, indicating the degree of velocity enhancement of colloid (i) relative to the conservative tracer (t), were calculated based on the effluent concentrations for $C_{Total-v}$, C_c, C_v, and C_{vc}. Furthermore, the mass recovery, M_r [–], of the tracer and the suspended $C_{Total-v}$, C_c, C_v particles, as well as the produced mass of C_{vc}, M_p [–], were quantified.

3.2. Filtration theory

The classical colloid filtration theory (CFT) was used to quantitatively compare the attachment of viruses and clay particles onto SWIs. The dimensionless collision efficiency, α [-], which represents the ratio of the collisions resulting in attachment to the total number of collisions between particles and collector grains [40], was calculated for the unsaturated transport experiments by the following expression [3,41]:

$$\alpha_{exp} = -\frac{2}{3}\frac{d_c}{L(1-\theta_m)\eta_0}\ln\left[\frac{C_{iss}}{C_{i0}}\right] \quad (1)$$

where θ_m [–] is the moisture content or volumetric water content (defined as the ratio of the liquid volume to the porous medium volume), d_c [L] is the mean collector diameter, C_{i0} [M/L^3] is the constant influent concentration of colloid i, C_{iss} [M/L^3] is the effluent colloid concentration of colloid i after the breakthrough curve has reached steady state conditions, and η_o [–] is the single-collector contact efficiency, which can be calculated from the relationship proposed by Tufenkji and Elimelech [42] by replacing θ with θ_m.

In this study, the suspended clay concentration was indicated by C_c [M/L^3]. Also, for the cotransport experiments conducted, the total virus concentration, $C_{Total-v}$ [M/L^3], was assumed to be equal to the effluent suspended virus concentration, C_v [M/L^3], plus the concentration of viruses attached onto suspended clay particles, C_{vc} [M/L^3]:

$$C_{Total-v} = C_v + C_{vc} \tag{2}$$

The tracer, virus, and clay initial concentrations were denoted by C_{t0} [M/L^3], C_{v0} [M/L^3], and C_{c0} [M/L^3], respectively; whereas, the concentrations of clay particles attached onto SWI and AWI were denoted by C_{c*} [M/M], and $C_c^{\diamond}$ [M/M], respectively. Using the concept of apparent collision efficiency, introduced by Walshe et al. [8] under saturated experimental conditions, two different apparent collision efficiencies were calculated. The first collision efficiency, $\alpha_{Total-v}$ [–], was based on $C_{Total-v}$ in the column effluent, which represents the attachment of C_v onto SWI, AWI, C_{c*}, and $C_c^{\diamond}$. The second collision efficiency, α_v [–], was based on C_v in the column effluent, which represents the attachment of both C_v and C_{vc}, onto SWI and AWI, denoted as C_{v*} [M/M], C_{vc*} [M/M], $C_v^{\diamond}$ [M/M], and $C_{vc}^{\diamond}$ [M/M], respectively, as well as the attachment of C_v onto C_c, C_{c*}, and $C_c^{\diamond}$, denoted as C_{vc}, C_{vc*}, and $C_{vc}^{\diamond}$, respectively. The various symbols used in this study are illustrated graphically in Fig. 1.

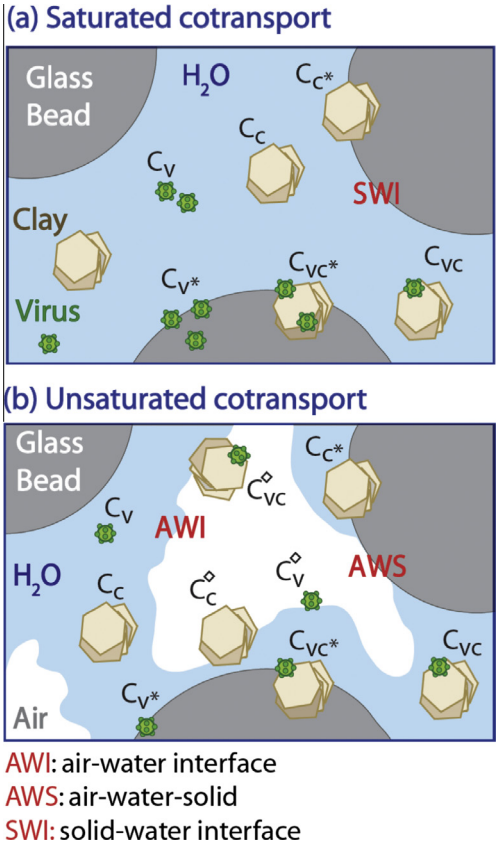

Fig. 1. Schematic illustration of the various concentrations involved in the cotransport experiments for: (a) saturated and (b) unsaturated porous media.

The collision efficiencies, $\alpha_{Total-v}$, and α_v for both MS2 and ΦX174 were calculated for the experimental conditions of this study using Eq. (1), where the η_0 values were obtained with the use of the following parameter values: complex Hamaker constant (virus-water collector and clay–water–collector) $A_{123} = 7.5 \times 10^{-21}$ kg m^2/s^2 [43], Boltzman constant $k_B = 1.38 \times 10^{-23}$ kg m^2/(s^2·K), fluid absolute temperature $T = 298$ K, particle diameter for MS2 $d_p = 2.5 \times 10^{-8}$ m, particle diameter for ΦX174 $d_p = 2.6 \times 10^{-8}$ m, particle density for MS2 $\rho_p = 1420$ kg/m^3 [8], particle density for ΦX174 $\rho_p = 1600$ kg/m^3 [44], particle density for clay colloids $\rho_p = 2200$ kg/m^3 [45], fluid density $\rho_f = 999.7$ kg/m^3, dynamic fluid viscosity $\mu_w = 8.91 \times 10^{-4}$ kg/(m·s), and acceleration due to gravity $g = 9.81$ m/s^2.

3.3. DLVO interaction energy calculations

To better understand the observed virus and clay colloid transport and deposition behavior in the unsaturated column experiments conducted in this study, the interaction energies between viruses-AWIs and clay particles-AWIs were calculated following the procedures described in Mitropoulou et al. [37], and compared with the interaction energy between viruses-SWIs and clay particles-SWIs reported by Syngouna and Chrysikopoulos [10]. The total interaction energy, Φ_{DLVO} [J], equals to the sum of the van der Waals, Φ_{vdW} [J], the electrostatic double layer, Φ_{dl} [J], and the Born, Φ_{Born} [J], interaction energies over the separation distance h [m] between the approaching surfaces. Note that the DLVO interaction energies were estimated by assuming that the colloid-air system can be represented by the ideal sphere-plate model, with Hamaker constant, A_{123}, for the (1-colloid)-(2-water)-(3-air) system estimated from the following expression [46]:

$$A_{123} = \left(\sqrt{A_{11}} - \sqrt{A_{22}}\right)\left(\sqrt{A_{33}} - \sqrt{A_{22}}\right) \tag{3}$$

where A_{11} [M·L^2/t^2] is the Hamaker constant of the colloid (clay or virus), A_{22} [M·L^2/t^2] is the Hamaker constant for the water, and A_{33} [M·L^2/t^2] is the Hamaker constant for the air. Unknown Hamaker constants can be calculated by the following geometric mixing rule:

$$A_{121} = \left(\sqrt{A_{11}} - \sqrt{A_{22}}\right)^2 \tag{4}$$

$$A_{11} = \left(\sqrt{A_{121}} + \sqrt{A_{22}}\right)^2 \tag{5}$$

In this study we employed previously measured values of A_{121} equal to 3.1×10^{-20} J, 2.5×10^{-20} J [47], and 0.97×10^{-20} J [48] for kaolinite, montmorillonite, and viruses, respectively, $A_{22} = 3.7 \times 10^{-20}$ J [46], and $A_{33} = 0$ J [46]. Hence, in view of Eq. (5), A_{11} was calculated equal to 1.36×10^{-19} J, 1.23×10^{-19} J and 0.85×10^{-19} J for kaolinite, montmorillonite, and viruses, respectively. The value of A_{123} for colloid–water–air systems was calculated by Eq. (3) equal to -3.39×10^{-20} J, -3.05×10^{-20} J, and -1.91×10^{-20} J for kaolinite, montmorillonite, and viruses, respectively. These negative values imply that the van der Waals interaction is repulsive for colloids at the AWI. Note that A_{123} can be negative when [49–51]:

$$A_{11} > A_{22} > A_{33} \tag{6}$$

or when:

$$A_{11} < A_{22} < A_{33} \tag{7}$$

It is not unusual to observe repulsive van der Waals forces. The London dispersion interactions between two molecules or particles (identical or different) in vacuum are always attractive. Also, London interactions between two identical molecules or particles immersed in a liquid are always attractive, except for the case

when $A_{11} = A_{22}$ where they are equal to zero (see Eq. (4)). However, when two different materials 1 and 3 interact, immersed in liquid 2, $A_{11} \neq A_{33}$, and the conditions in Eq. (6) or Eq. (7) prevail, a net repulsion occurs.

3.4. Capillary energy calculations

In unsaturated porous media, colloid capillary retention refers to deposition of colloids due to capillary force interactions. Note that the capillary and associated friction forces are instrumental to the retention of colloids within water films and at AW_mS interfaces [26]. If the thickness of an adsorbed water film, h_f [L], is smaller than the colloid diameter d_p [L], film straining occurs [26,29,52–54].

A capillary force, F_c [M·L/t^2], acting on a colloid trapped in a thin water film at the contact line can be decomposed into two forces: one parallel (laterally around the colloid), F_{pc} [M·L/t^2], and one perpendicular (vertical), F_{vc} [M·L/t^2], to the glass bead surface, as shown in Fig. 2. Note that the capillary force components parallel to the glass bead are perfectly balanced so that the net parallel force is equal to zero. When the colloid is in contact with the glass bead surface (i.e., at $h = 0.3$ nm), the DLVO force, F_{DLVO}, is attractive, as shown in Fig. 2. Note that F_{DLVO} does not depend on the filling angle, φ [°], between the center of the colloid and the water colloid contact line (see Fig. 2). If $h > 0.3$ nm, then the attractive DLVO force would decrease considerably. For simplicity the glass bead surface is assumed to be flat because both viruses and clays are much smaller than the glass bead. Consequently, a spherical colloid with radius r_p [L], trapped within a water film with height h_f, is held against the glass bead surface by the total vertical capillary force $F_{v\text{-}tot}$, which can be expressed as follows [26]:

$$F_{v-tot} = \sigma_{aw} 2\pi \sqrt{r_p^2 - (h_f - r_p)^2} \cos\left[\beta + \frac{\pi}{2} - \cos^{-1}\left(\frac{h_f - r_p}{r_p}\right)\right] \quad (8)$$

where σ_{aw} [M/t^2] is the air–water surface tension ($\sigma_{aw} = 0.0718$ N/m at 25 °C), β [°] is the contact angle between the water and the colloid. The above expression is valid only for $h_f \leqslant 2r_p$. When the film thickness is larger than the colloid diameter ($h_f > 2r_p$), the film is not distorted. Furthermore, when $h_f > r_p(1 + \cos\beta)$ the capillary force direction is away from the glass bead surface, and the capillary potential is negative [26]. Assuming that the net lateral capillary force is zero ($F_{pc} = 0$), colloids trapped in the water film will be immobile as long as the meniscus is not moving. Furthermore, F_{vc} induces a friction force on the glass bead, which can prevent colloids from moving even if film flow exerts a drag force on the colloids. It is worthy to note that F_c values are reported to be at least two orders of magnitude greater than typical F_{DLVO} values [23,26,28].

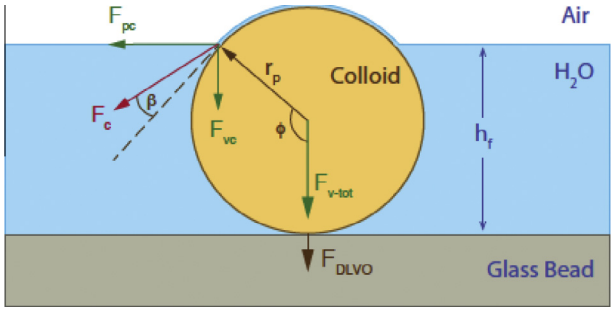

Fig. 2. Schematic illustration of a colloid with radius r_p, in contact with a glass bead, trapped in a thin water film with thickness h_f. A capillary force F_c with components F_{pc} and F_{vc}, is acting on the colloid at the contact line with contact angle β. The F_{pc} components are perfectly balanced laterally around the colloid; whereas the F_{vc} components yield the total vertical capillary force $F_{v\text{-}tot}$. Also shown is the attractive F_{DLVO}, which is not dependent on the filling angle ϕ.

The capillary potential energy, Φ_c [J], for a colloid that protrudes a distance, d_f [L], out of either a film or AW_mS, can be determined by integrating the capillary force over its path in the direction of the force through the water film as follows [26]:

$$\Phi_c = \int_{z=r_p(1-\cos\beta)}^{z=d_f} F_{v-tot}\,dz = \int_{z=r_p(1-\cos\beta)}^{z=d_f} \sigma_{aw} 2\pi \sqrt{r_p^2 - (r_p - z)^2} \cos\left[\beta + \frac{\pi}{2} - \cos^{-1}\left(\frac{r_p - z}{r_p}\right)\right] dz \quad (9)$$

where z is a selected coordinate that passes through the colloid center and is orthogonal to the original meniscus. The latter formulation in Eq. (9) is a consequence of employing Eq. (8) with $h_f = 2r_p - z$. Note that $z = 0$ is at the surface of the colloid, and $z = r_p(1 - \cos\beta)$ is where the net force on the colloid is zero. To analyze the relative importance of capillary forces for colloid retention at the thin water film, Φ_c for both clay colloids and viruses were calculated using Eq. (9), and compared with those calculated based on the DLVO theory, Φ_{DLVO} [J]. In this study, the following colloid water contact angles were employed: $\beta_{MS2} = 33 \pm 1°$, $\beta_{\Phi X174} = 26 \pm 1.7°$ [55], $\beta_{KGa\text{-}1b} = 46.1°$, and $\beta_{STx\text{-}1} = 20.5 \pm 2.8°$ [56].

4. Results and discussion

4.1. Transport experiments

Fig. 3 presents the normalized breakthrough data collected from the transport experiments with tracer, viruses (MS2 and ΦX174), and clay particles (KGa-1b, STx-1b) as a function of pore volume, under unsaturated (Fig. 3a–e) and saturated (Fig. 3f–j) conditions. The corresponding M_r values for all the transport experiments are listed in Table 1. The experimental results suggested that peak concentrations and mass recoveries for all of the viruses and clay colloids employed, increased with increasing saturation level, S_w [–]. Generally, MS2 exhibits poorer attachment to solid surfaces, presumably due to its lower isoelectric point [57], and ΦX174 possesses fewer negative charges than MS2 at the experimental pH conditions of this study [58]. Thus, ΦX174 was attached onto the solid matrix more than MS2. This observation contradicts our previous experimental results obtained under saturated transport conditions with identical specific discharge [10,59]. Note that ΦX174 is less hydrophobic than MS2 [57]. Hydrophobic interactions could become increasingly important during virus filtration. Moreover, enhanced repelling forces due to the intrinsic steric stabilization of phage ΦX174, induced by the knobs found on its capsid, could also explain the increased retention observed for MS2 relative to ΦX174 [48]. Although low M_r values cannot lead to the conclusion that virus particles retained were irreversibly attached or inactivated, the possibility that the observed low M_r values are caused by irreversible attachment and inactivation cannot be ruled out. With the only exception of ΦX174 under the saturated experimental conditions, velocity enhancement (early breakthrough) was observed ($M_{1(i)}/M_{1(t)} > 1$) for all cases examined (see Table 1). Note that higher velocity enhancement for all of the viruses and clays compared to the tracer was observed under unsaturated than saturated experimental conditions.

The M_r values, listed in Table 1, indicated that the saturation level significantly affected the retention of viruses and clay colloids by the packed column. Moreover, higher M_r values were observed for STx-1b than KGa-1b under both saturated and unsaturated experimental conditions. The higher retention observed for

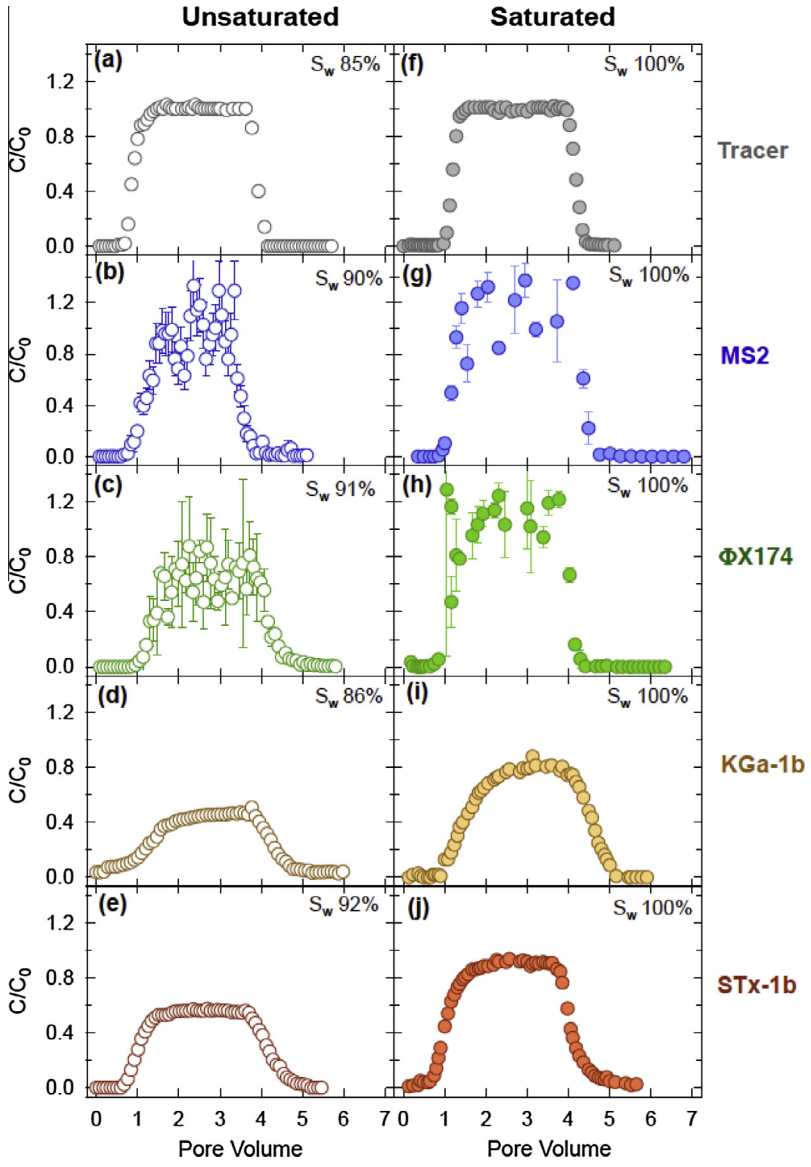

Fig. 3. Breakthrough data from the transport experiments with tracer, viruses (MS2, ΦX174), and clays (KGa-1b, STx-1b) in unsaturated (a–e: open symbols), and saturated (f–j: filled symbols) columns packed with glass beads.

KGa-1b could be attributed to its higher hydrophobicity compared to that of STx-1b [35].

4.2. Cotransport experiments

Fig. 4 presents the normalized breakthrough data collected from cotransport experiments with ΦX174 and clay (KGa-1b, STx-1b) as a function of pore volume, under both saturated and unsaturated conditions. The corresponding M_r and M_p values for all the cotransport experiments are listed in Table 1. Note that the M_r values for ΦX174 based on $C_{Total-v}$ in the effluent, were considerably reduced in the presence of clay particles, compared to the M_r values obtained in the absence of clay particles (see Table 1). This is attributed to the clay-bound viruses, which were retained in the column due to clay attachment onto the glass beads [9,10]. Moreover, M_r values calculated based on $C_{Total-v}$, C_v, and C_c, as well as M_p values calculated based on C_{vc}, were observed to be higher under saturated than unsaturated conditions. Furthermore, the ratios $M_{1(i)}/M_{1(t)}$ calculated for ΦX174 based on $C_{Total-v}$, C_v, and C_{vc} (see Table 1) suggested that the transport of ΦX174 is hindered by the presence of KGa-1b under saturated conditions ($M_{1(i)}/M_{1(t)}$ values follow the trend $C_{vc} < C_{Total-v} < C_v < 1$), while the transport of ΦX174 is facilitated by the presence of STx-1b under saturated conditions ($M_{1(i)}/M_{1(t)}$ values follow the trend $C_{vc} > 1$ and $C_{Total-v} < C_v < 1$). Worthy to note is that, under unsaturated conditions, both clay particles facilitate the transport of ΦX174 ($M_{1(i)}/M_{1(t)}$ values follow the trend $C_{vc} > C_{Total-v} > C_v > 1$).

Fig. 5 shows the normalized breakthrough data collected from the cotransport experiments with MS2 and clay (KGa-1b, STx-1b) as a function of pore volume, under both saturated and unsaturated conditions. The corresponding M_r and M_p values for all the cotransport experiments are listed in Table 1. The various $M_{1(i)}/M_{1(t)}$ ratios calculated for MS2 based on $C_{Total-v}$, C_v and C_{vc} listed in Table 1, indicated that under saturated conditions, KGa-1b hindered ($M_{1(i)}/M_{1(t)}$ values follow the trend $C_{vc} < C_{Total-v} < C_v < 1$), while STx-1b facilitated ($M_{1(i)}/M_{1(t)}$ values follow the trend $C_{Total-v} < C_v < C_{vc} < 1$) the transport of MS2. Similarly, Jin et al. [60] found that sodium-saturated montmorillonite greatly enhanced MS2 transport through saturated sand columns. Conceivably, suspended STx-1b particles could absorb both MS2

Table 1
Experimental conditions and estimated parameters.

Experiment	Initial concentration	θ (–)	θ_m (–)	S_w (–)	U (cm/min)	M_r (%)		M_p (%) for C_{vc}	$M_{1(i)}/M_{1(t)}$			$\alpha_{Total-v}$ (–)	α_v (–)
						for $C_{Total-v}$ or C_c	for C_v		for $C_{Total-v}$ or C_c	for C_v	for C_{vc}		
Transport experiments													
Tracer	0.01 mol/L	0.42	–	1.00	0.74	100.0	–	–	1.00	–	–	–	–
Tracer	0.01 mol/L	0.41	0.38	0.93	0.66	111.0	–	–	1.00	–	–	–	–
ΦX174	3817 PFU/mL	0.42	–	1.00	0.74	100.0	–	–	0.90	–	–	0.00	–
ΦX174	3450 PFU/mL	0.41	0.38	0.91	0.66	64.9	–	–	1.31	–	–	0.13	–
MS2	4842 PFU/mL	0.42	–	1.00	0.74	100	–	–	1.00	–	–	0.00	–
MS2	13,150 PFU/mL	0.42	0.38	0.90	0.58	76.6	–	–	1.26	–	–	0.08	–
KGa-1b	67.6 mg/L	0.42	–	1.00	0.74	79.5	–	–	1.10	–	–	0.15	–
KGa-1b	69.28 mg/L	0.40	0.38	0.86	0.70	49.3	–	–	1.23	–	–	0.70	–
STx-1b	102.3 mg/L	0.42	–	1.00	0.74	93.8	–	–	1.00	–	–	0.03	–
STx-1b	88.06 mg/L	0.41	0.38	0.92	0.69	59.1	–	–	1.26	–	–	0.35	–
Cotransport experiments													
ΦX174–KGa-1b	(2767 PFU/mL)–(80.8 mg/L)	0.42	–	1.00	0.74	(64.6) –(27.2)	43.4	21.6	(0.82)–(0.87)	0.83	0.79	(0.08) –(0.86)	0.15
ΦX174–KGa-1b	(5100 PFU/mL)–(75.0 mg/L)	0.42	0.39	0.92	0.64	(30.6) –(40.6)	18.7	12.0	(1.01)–(1.13)	1.01	1.02	(0.18) –(1.00)	0.37
ΦX174–STx-1b	(4817 PFU/mL)–(122.2 mg/L)	0.42	–	1.00	0.74	(71.9) –(47.7)	43.0	27.2	(0.79)–(0.77)	0.82	1.01	(0.06) –(0.29)	0.15
ΦX174–STx-1b	(7433 PFU/mL)–(107.0 mg/L)	0.45	0.37	0.83	0.72	(53.5) –(25.1)	37.3	16.2	(1.11)–(1.18)	1.08	1.18	(0.18) –(0.83)	0.29
MS2–KGa-1b	(9767 PFU/mL)–(77.0 mg/L)	0.42	–	1.00	0.74	(53.8) –(31.4)	40.0	14.7	(0.78)–(0.85)	0.85	0.70	(0.11) –(0.77)	0.16
MS2–KGa-1b	(21,383 PFU/mL)–(69.0 mg/L)	0.43	0.37	0.83	0.72	(52.2) –(28.6)	25.8	26.0	(1.08)–(1.01)	1.20	0.96	(0.17) –(1.00)	0.36
MS2–STx-1b	(9500 PFU/mL)–(92.6 mg/L)	0.42	–	1.00	0.74	(67.7) –(42.9)	38.5	35.1	(0.89)–(0.85)	0.92	0.93	(0.07) –(0.33)	0.17
MS2–STx-1b	(11,067 PFU/mL)–(89.0 mg/L)	0.43	0.35	0.81	0.70	(70.0) –(22.0)	43.4	27.9	(1.09)–(1.12)	1.00	1.06	(0.09) –(0.85)	0.21

and ΦX174 viruses and facilitate their transport. The higher outflow of $C_{Total-v}$ and C_{vc} concentrations observed in the presence of STx-1b than KGa-1b under saturated conditions could be attributed to the higher M_r values estimated for STx-1b than KGa-1b (see Figs. 4 and 5). Note that STx-1b is less hydrophobic than KGa-1b [35]. Also, the virus adsorption mechanism can vary for different viruses and can be affected significantly by the clay characteristics. In contrast to the experimental results for the case of ΦX174 cotransport, both clay particles hinder the transport of MS2 under unsaturated conditions. Note that for virus transport, mobilization and attachment onto clay colloids under unsaturated conditions, as well as the balance among electrostatic, hydrodynamic, and capillary forces are responsible for attraction of viruses toward the AWI [61,62]. A moving AWI tends to dominate colloid movement during water infiltration into porous media [61]. However, under steady-state flow conditions a stationary AWI is expected [63]. The strong force associated at the AWI can overcome colloid aggregation and settling, which otherwise dominate colloid dispersion and mobility in porous media. Moreover, in the presence of viruses (MS2, ΦX174), the transport of KGa-1b and STx-1b was shown to be retarded under water saturated conditions ($M_{1(i)}/M_{1(t)}$<1 based on C_c), and enhanced under water unsaturated conditions ($M_{1(i)}/M_{1(t)}$>1 based on C_c) compared to the tracer (see Table 1).

The various M_r and M_p values calculated for ΦX174, MS2, KGa-1b, and STx-1b are illustrated graphically in Fig. 6. In the presence of STx-1b, the M_p values based on C_{vc} for both viruses were higher than those in the presence of KGa-1b under both saturated and unsaturated conditions. Furthermore, with the only exception of MS2-KGa-1b cotransport, the various M_r values listed in Table 1 indicated that by increasing the saturation level, the difference between $C_{Total-v}$ and C_v for both viruses also increased, suggesting that more viruses were attaching onto suspended clay colloids. The possibility that C_v and C_{vc} inactivation is not identical should not be eliminated. However, it has been reported in the literature that the inactivation rate of C_v and C_{vc} in batch experiments is quite similar [33,59]. Moreover, it has been reported in the literature that inactivation rates for adsorbed and non-adsorbed viruses onto the solid matrix of the porous media: C_v, C_{v*} and $C_v^{\diamond}$ are different [64–68]. Consequently, it is quite reasonable to assume that the inactivation rates for adsorbed and non-adsorbed virus-clay colloid clusters C_{vc}, C_{vc}^{*} and $C_{vc}^{\diamond}$ are different. Also, the presence of viruses affected C_c transport because the M_r values of both KGa-1b and STx-1b were substantially reduced in the presence of both viruses compared to the case of C_c transport in the absence of viruses, under both saturated and unsaturated conditions (see Table 1). The M_r values for both KGa-1b and STx-1b based on C_c, in most cases examined, were lower under unsaturated than saturated conditions.

4.3. Collision efficiencies

The collision efficiency values $\alpha_{Total-v}$, based on $C_{Total-v}$, and α_v values based on C_v, as calculated with Eq. (1), are graphically presented in Fig. 7, and are listed in Table 1. The $\alpha_{Total-v}$ holds information about the adsorption of $C_{Total-v}$ onto SWI and AWI (transport experiments), and the adsorption of $C_{Total-v}$ onto both SWI, AWI and clay colloids previously attached onto SWI (C_{c*}) and AWI ($C_c^{\diamond}$) (cotransport experiments). The $\alpha_{Total-v}$ values for ΦX174 in the transport experiments were higher than those for MS2 only under unsaturated conditions (see Table 1). In the presence of clay colloids (cotransport experiments), the $\alpha_{Total-v}$ values were higher for both viruses in all cases examined, which indicated that more attachment sites were available on the solid matrix (SWI, AWI, C_{c*} and $C_c^{\diamond}$) than in the absence of clay colloids. In the presence of both KGa-1b and STx-1b, the $\alpha_{Total-v}$ values increased with decreasing saturation level. Furthermore, the

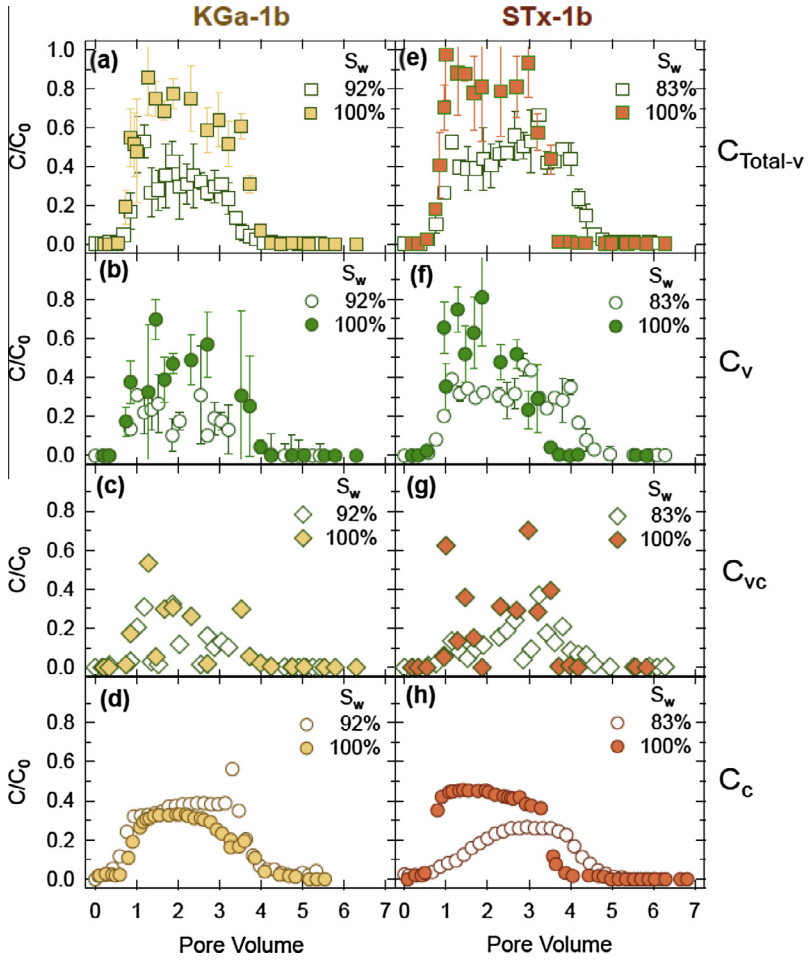

Fig. 4. Breakthrough data from the cotransport experiments with: (a–d) ΦX174-KGa-1b, and (e–h) ΦX174-STx-1b in saturated (filled symbols), and unsaturated (open symbols) columns packed with glass beads. The concentrations $C_{Total-v}$ are presented in (a and e), C_v in (b and f), C_{vc} in (c, g), and C_c in (d and h).

relative high α_v values ($\alpha_v > \alpha_{Total-v}$ shown in Table 1) indicated that the presence of clay colloids increased the attachment of viruses onto SWI, AWI, and clay colloids. In all cases examined, the α_v values increased with decreasing saturation level. Note that the CFT assumes that the column packing is clean, and that deposited colloids do not affect the rate of colloid removal [39,41]. If a collector becomes partly blocked by the presence of attached viruses and clay colloids, the overall $\alpha_{Total-v}$ and α_v may either increase or decrease when additional viruses and clay colloids are added, depending on whether clay–clay, virus–virus and clay–virus attachment is favorable or unfavorable [8]. Higher α_v values were observed for MS2 than ΦX174 in the presence of both KGa-1b and STx-1b only under saturated experimental conditions, which could be attributed to the greater affinity of MS2 for both clay particles [35]. Note that exactly the opposite is observed (higher α_v values for ΦX174 than MS2) in the presence of both clays under unsaturated conditions, which indicates that AWI plays a significant role on MS2 attachment and inactivation. This observation is in agreement with the experimental results of previous studies [69,70].

4.4. DLVO and Capillary Energy Profiles

The total Φ_{DLVO} interaction energy, according to the DLVO theory, for the experimental conditions of this study (pH = 7, I_s = 0.1 mM) have been previously estimated for colloid–colloid (sphere-plate for virus-clay, sphere–sphere for virus–virus and clay–clay) interactions by Chrysikopoulos and Syngouna [35], and for colloid-SWI (sphere-plate for virus-SWI and clay-SWI) interactions by Syngouna and Chrysikopoulos [10]. Furthermore, The total Φ_{DLVO} interaction energy calculations for colloid-AWI (sphere-plate for virus-AWI and clay-AWI) interactions are presented in Fig. 8. Also, all the estimated Φ_{min1}, Φ_{min2} and Φ_{max1} values of the various DLVO energy curves are listed in Table 2. Fig. 8 shows that virus attachment onto AWIs was not favorable. Furthermore, given that the A_{123} for colloids interacting with AWIs was found to be negative, the dielectric constant and the refractive index of air are equal to 1, the resulting van der Waals interaction energies are repulsive, and in turn the total interaction energies, Φ_{DLVO}, for the two viruses with AWIs are repulsive for all separation distances. It should be noted that no Φ_{min2} exists for virus-AWI interactions under the experimental conditions. Moreover, Φ_{min1} exists only for the case of ΦX174, while permanent retention of MS2 at AWIs cannot be expected under the experimental conditions of this study (Φ_{min1} for MS2 does not exist). Note that, the calculated virus DLVO energy profiles are in agreement with the observed lower mass recovery values for ΦX174 compared to MS2 under unsaturated conditions (see Table 1, Fig. 6). Furthermore, a Φ_{min1} was observed in the interaction energy profiles for the two clays with AWIs, which suggests that clays could adhere onto AWIs if they have sufficient kinetic energy to overcome the potential energy barrier.

Fig. 9 shows the capillary energy potentials Φ_c of the clay colloids (KGa-1b, STx-1b) and viruses (MS2, ΦX174) calculated with Eq. (9) for different d_f distances from the meniscus. Based on Eq. (9), $\Phi_c = 0$ for MS2 (with $\beta_{MS2} = 26°$) $h_f = 1.89 r_p$. For ΦX174

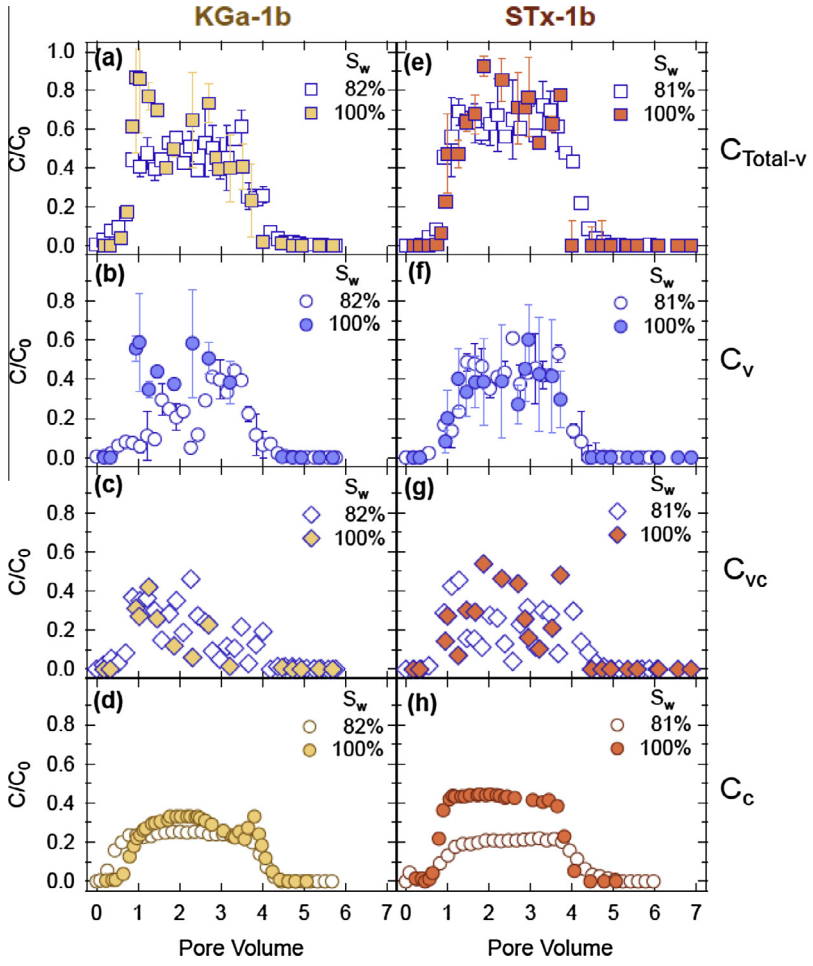

Fig. 5. Breakthrough data from the cotransport experiments with: (a–d) MS2-KGa-1b, and (e–h) MS2-STx-1b in saturated (filled symbols), and unsaturated (open symbols) columns packed with glass beads. The concentrations $C_{Total-v}$ are presented in (a and e), C_v in (b and f), C_{vc} in (c and g), and C_c in (d and h).

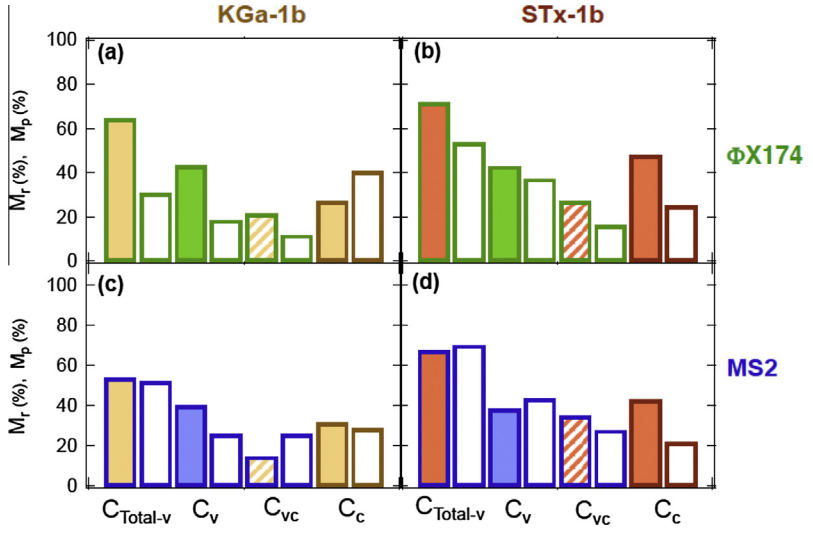

Fig. 6. Calculated mass recovery values based on $C_{Total-v}$, C_v and C_c, and calculated mass produced values based on C_{vc}, from the cotransport experiments with: (a) ΦX174 and KGa-1b, (b) ΦX174 and STx-1b, (c) MS2 and KGa-1b, and (d) MS2 and STx-1b under saturated (filled columns) and unsaturated (open columns) conditions.

(with $\beta_{\Phi X174} = 33°$), Eq. (9) yields that $\Phi_c = 0$ when $h_f = 1.84r_p$. For KGa-1b (with $\beta_{KGa\text{-}1b} = 46.1°$) Eq. (9) yields that $\Phi_c = 0$ when $h_f = 1.69r_p$. For STx-1b ($\beta_{STx\text{-}1} = 20.5°$), Eq. (9) yields that $\Phi_c = 0$ when $h_f = 1.94r_p$. Moreover, Fig. 9 clearly shows that when $h_f \to 0$ (or $d_f \to 2r_p$) the capillary potential energy Φ_c increases to values ranging from 10^4 k_BT (for viruses, see Fig. 9b) to 10^7 k_BT (for clay colloids, see Fig. 9a). Note that the capillary potential is lower for more hydrophobic colloids ($\Phi_{c(MS2)} < \Phi_{c(\Phi X174)}$, $\Phi_{c(KGa\text{-}1b)} < \Phi_{c(STx\text{-}1b)}$) when they both protrude through the film by the same distance (see Fig. 9). Therefore, greater capillary retention occurs in the

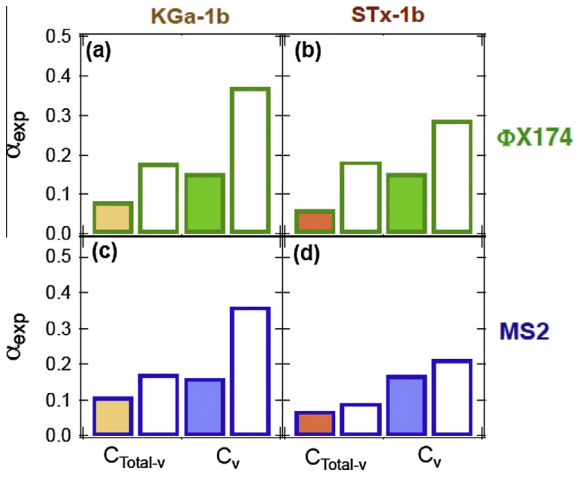

Fig. 7. Experimental collision efficiencies calculated with the effluent concentrations $C_{Total-v}$ and C_v obtained from the cotransport experiments with: (a) ΦX174 and KGa-1b, (b) ΦX174 and STx-1b, (c) MS2 and KGa-1b, and (d) MS2 and STx-1b under saturated (filled columns) and unsaturated (open columns) conditions.

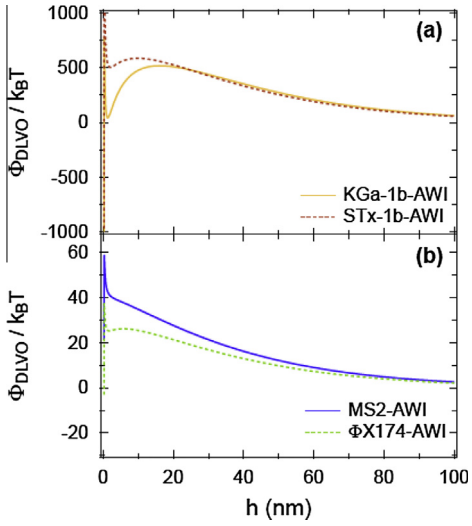

Fig. 8. Predicted DLVO energy interactions as a function of separation distance, based on the sphere-plate model for: (a) KGa-1b-AWI, STx-1b-AWI, and (b) MS2-AWI, ΦX174-AWI.

Table 2
Various estimated values of Φ_{min1}, Φ_{min2} and Φ_{max1}.

Interacting pair	Φ_{min1} (k_BT)	Φ_{max1} (k_BT)	Φ_{min2} (k_BT)	Refs.
MS2–SWI	na	33.5	−0.00011	[10]
MS2–MS2	na	na	−0.0115	[35]
MS2–AWI	na	58.92	na	This study
MS2–KGa-1b	na	14.7	−0.0012	[35]
MS2–STx-1b	−5.8	9.8	−0.0014	[35]
ΦX174–SWI	na	23.3	−0.00011	[10]
ΦX174–ΦX174	na	na	−0.108	[35]
ΦX174–AWI	−3.05	37.51	na	This study
ΦX174–KGa-1b	na	13.2	−0.0013	[35]
ΦX174–STx-1b	−2.4	9.3	−0.0014	[35]
KGa-1b–SWI	−163	1072	−0.0038	[10]
KGa-1b–KGa-1b	na	na	−0.6136	[35]
KGa-1b–AWI	−969.5	586.2	na	This study
STx-1b–SWI	−1438	973.5	−0.0057	[10]
STx-1b–STx-1b	na	10.7	−0.7639	[35]
STx-1b–AWI	−2213	517.4	na	This study

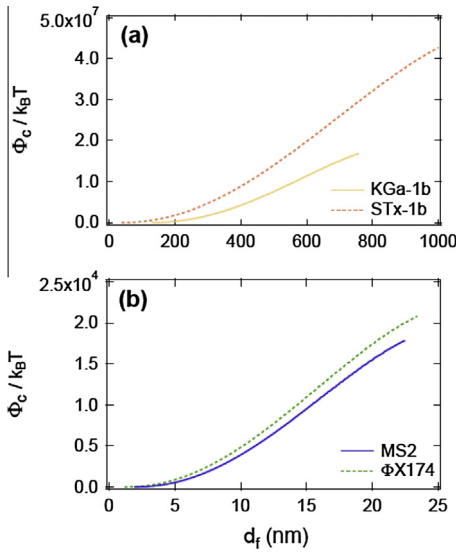

Fig. 9. Calculated capillary potential energy Φ_c as a function of d_f for: (a) clay colloids (KGa-1b, STx-1b), (b) and viruses (MS2, ΦX174) retained within thin water films and at AW_mS interfaces.

presence of hydrophilic colloids compared to relatively hydrophobic colloids [24,26].

The Φ_{DLVO} for colloid-SWI interactions for separation distances of 1.7, 4, 7, 11 nm have been reported in the literature to be 33.5, 23.3, 1072, 973.5 k_BT for MS2, ΦX174, KGa-1b, and STx-1b with glass beads, respectively [10] (see Table 2). At separation distances less than those above, the particles become attractive because of the van der Waals forces. Thus, the Φ_c potential energy is several orders of magnitude greater than the Φ_{DLVO} potential energy (see Fig. 9). Note that, capillary potential forces are much greater than the electric double layer repulsive forces and can push the colloid close enough to the grain surface where colloids are attracted to the collector through van der Waals forces [26].

5. Summary and Conclusions

In this study, the effects of clay colloids, and water saturation level on virus transport in porous media were examined. It was shown that the water saturation level had the greatest relative impact on virus-clay colloid cotransport. In most cases, the fraction of viruses attached onto clay colloids decreased with a decreasing saturation level. The data from the cotransport experiments under water-saturated conditions revealed that KGa-1b hindered while STx-1b facilitated the transport of both MS2 and ΦX174. Worthy to note is that, under unsaturated conditions, clay colloids (KGa-1b, STx-1b) facilitated the transport of ΦX174 while hindered the transport of MS2. Also, in the presence of viruses, the transport of KGa-1b and STx-1b was retarded under water saturated conditions, and enhanced under water unsaturated conditions, compared to the tracer.

The total Φ_{DLVO} interaction energy calculations for the various virus-AWI revealed that permanent retention of ΦX174 at AWIs can be expected under the experimental conditions of this study (Φ_{min1} exists). Furthermore, a Φ_{min1} was observed in the interaction energy profiles for the clays with AWIs, which suggests that clays could adhere onto AWIs, if they have sufficient kinetic energy to overcome the potential energy barrier. Moreover, Φ_c is several orders of magnitude greater than Φ_{DLVO} as a function of the distance of the colloid to the SWI. Note that the capillary potential is lower for MS2 than ΦX174, and lower for KGa-1b than STx-1b for identical d_f value.

Acknowledgments

This research has been co-financed by the European Union (European Social Fund-ESF) and Greek National Funds through the Operational program "Education and Lifelong Learning" under the action Aristeia I (Code No. 1185). This work is a collaboration between members of the BioMet Network.

Appendix A. Nomenclature

A_{123}	Hamaker constant ($M{\cdot}L^2/t^2$)
C_c	suspended clay particle concentration (M/L^3)
C_{iss}	effluent suspended clay particle concentration at steady state conditions (M/L^3)
C_{c*}	Concentration of clay particles irreversibly attached onto SWI (M/M)
$C_c^{\diamond}$	Concentration of clay particles captured in AWI (M/M)
Ci_o	constant influent concentration of colloid i (M/L^3)
C_{to}	tracer initial concentration (M/L^3)
$C_{Total-v}$	total virus concentration (M/L^3)
C_v	suspended virus concentration in liquid phase (M/L^3)
C_{v*}	concentration of viruses attached onto SWI (virus mass/solid mass) (M/M)
$C_v^{\diamond}$	concentration of viruses captured in AWI (M/M)
C_{vc}	concentration of viruses attached onto suspended clay particles (M/M)
C_{vc*}	concentration of viruses attached onto clay particles previously deposited onto SWI (M/M)
$C_{vc}^{\diamond}$	concentration of viruses attached onto clay particles previously deposited onto AWI (M/M)
d_c	collector diameter (L)
d_f	distance that a colloid protrudes out from a thin water film (L)
d_p	average colloidal particle diameter (L)
F_c	capillary force (N) ($M{\cdot}L/t^2$)
F_{pc}	lateral component of the capillary force (N) ($M{\cdot}L/t^2$)
F_{vc}	vertical component of the capillary force(N) ($M{\cdot}L/t^2$)
$F_{v\text{-}tot}$	total vertical capillary force (N) ($M{\cdot}L/t^2$)
g	acceleration due to gravity (L/t^2)
h	separation distance between two approaching surfaces (L)
h_f	water film thickness (L)
i	subscript indicating the various colloids used in this study (–)
I_s	ionic strength (mol/L)
k_B	Boltzman's constant ($M{\cdot}L^2/(t^2{\cdot}K)$)
L	length of packed column (L)
M_1	first normalized temporal moment (t)
$M_{r(i)}$	mass recovery in the outflow of species i (–)
$M_{p(i)}$	mass production in the outflow of species i (–)
N_A	Avogadro's number (1/mol)
q	specific discharge (Darcian fluid flux) (L/t)
r_p	colloidal particle radius (L)
S_w	degree of saturation (–)
t	time (t)
T	Temperature (K) (T)
U	average interstitial velocity (L/t)
x	Cartesian coordinate (L)
Greek letters	
α	collision efficiency (–)
α_{exp}	experimental collision efficiency (–)
$\alpha_{Total-v}$	apparent collision efficiency based on the $C_{Total-v}$ in the effluent (–)
α_v	apparent collision efficiency based on the C_v in the effluent (–)
β	contact angle of the water surface with the colloid (°)
ζ	electrokinetic zeta potential (V)
η_0	single-collector removal efficiency for favorable deposition (–)
θ	porosity (voids volume to porous medium volume) (L^3/L^3)
θ_m	moisture content or volumetric water content (liquid volume to porous medium volume) (L^3/L^3)
λ	inactivation rate coefficient of suspended viruses (1/t)
λ^*	inactivation rate coefficient of sorbed viruses at the SWI (1/t)
$\lambda^{\diamond}$	inactivation rate coefficient of sorbed viruses at the AWI (1/t)
μ_w	dynamic fluid viscosity (M/(L·t)
ρ_b	bulk density of the solid matrix (solids mass/aquifer volume) (M/L^3)
ρ_f	fluid density (M/L^3)
ρ_p	colloidal particle density (M/L^3)
σ_{aw}	air-water interfacial tension (M/t^2)
φ	filling angle between the center of the colloid and the water colloid contact line (°)
Φ_{Born}	Born potential energy (J) ($M{\cdot}L^2/t^2$)
Φ_c	capillary potential energy (J) ($M{\cdot}L^2/t^2$)
Φ_{dl}	double layer potential energy (J) ($M{\cdot}L^2/t^2$)
Φ_{DLVO}	DLVO potential energy (ML^2/t^2)
Φ_{max1}	primary maximum of the total interaction energy (J) ($M{\cdot}L^2/t^2$)
Φ_{min1}	primary minimum of total interaction energy (J) ($M{\cdot}L^2/t^2$)
Φ_{min2}	secondary minimum of total interaction energy (J) ($M{\cdot}L^2/t^2$)
Φ_{vdW}	van der Waals potential energy (J) ($M{\cdot}L^2/t^2$)
Ψ_p	surface potential of the colloid particle (V)
Abbreviations	
AWI	air–water interface
AWS	air–water–solid
AW_mS	air–water meniscus–solid
CFT	colloid filtration theory
ddH_2O	deionized distilled water
DLVO	Derjaguin–Landau–Verwey–Overbeek
SWI	solid–water interface

References

[1] A. Abdel-Salam, C.V. Chrysikopoulos, Adv. Water Resour. 17 (5) (1994) 283–296, http://dx.doi.org/10.1016/0309-1708(94)90032-9.
[2] J.E. Saiers, G.M. Hornberger, Water Resour. Res. 32 (1996) 33–41.
[3] R. Kretzschmar, M. Borkovec, D. Grolimund, M. Elimelech, Adv. Agron. 66 (1999) 121–194.
[4] M.E. Tatalovich, K.Y. Lee, C.V. Chrysikopoulos, Transp. Porous Media 38 (2000) 93–115, http://dx.doi.org/10.1023/A:1006674114600.
[5] S.C. James, T.K. Bilezikjian, C.V. Chrysikopoulos, Stochastic Environ. Res. Risk Assess. 19 (2005) 266–279, http://dx.doi.org/10.1007/s00477-004-0231-3.
[6] L. Pang, M. Noonan, M. Flintoft, P. van den Brink, J. Environ. Qual. 34 (2005) 237–247.
[7] G. Severino, V. Cvetkovic, A. Coppola, Adv. Water Resour. 30 (2007) 101–112.
[8] G.E. Walshe, L. Pang, M. Flury, M.E. Close, M. Flintoft, Water Res. 44 (2010) 1255–1269.
[9] I.A. Vasiliadou, C.V. Chrysikopoulos, Water Resour. Res. 47 (2011) W02543, http://dx.doi.org/10.1029/ 2010WR009560.
[10] V.I. Syngouna, C.V. Chrysikopoulos, Colloids Surf. A: Physicochem. Eng. Aspects 416 (2013) 56–65, http://dx.doi.org/10.1016/j.colsurfa.2012.10.018.
[11] V.E. Katzourakis, C.V. Chrysikopoulos, Adv. Water Resour. 68 (2014) 62–73, http://dx.doi.org/10.1016/j.advwatres.2014.03.001.
[12] J.M. Wan, J.L. Wilson, Water Resour. Res. 30 (1994) 11–23.
[13] M.Y. Corapcioglu, H. Choi, Water Resour. Res. 32 (1996) 3437–3449.
[14] J.M. Wan, T.K. Tokunaga, Environ. Sci. Technol. 31 (1997) 2413–2420.
[15] A. Schäfer, H. Harms, A.J.B. Zehnder, Environ. Sci. Technol. 32 (1998) 3704–3712.
[16] Y. Chu, Y. Jin, M. Flury, M.V. Yates, Water Resour. Res. 37 (2) (2001) 253–263.
[17] G. Chen, M. Flury, Colloids Surf. A: Physicochem. Eng. Aspects 256 (2005) 207–216. Corrections, Colloids Surf. A: Physicochem. Eng.Aspects 289 (2006) 254-255; Colloids Surf. A: Physicochem. Eng. Aspects, 396(2012) 352–353.
[18] S. Torkzaban, S.A. Bradford, M.Th. van Genuchten, S.L. Walker, J. Contam. Hydrol. 96 (2008) 113–127.
[19] G. Chen, S.L. Walker, Environ. Sci. Technol. 46 (2012) 8782–8790.
[20] Y. Sim, C.V. Chrysikopoulos, Colloids Surf. Physicochem. Eng. Aspects 155 (1999) 189–197, http://dx.doi.org/10.1016/S0927-7757(99)00073-4.
[21] Y. Sim, C.V. Chrysikopoulos, Water Resour. Res. 36 (2000) 173–179, http://dx.doi.org/10.1029/1999WR900302.
[22] R. Anders, C.V. Chrysikopoulos, Transp. Porous Media 76 (2009) 121–138. 10.1007/s11242-008-9239-3.
[23] W. Zhang, V.L. Morales, M.E. Cakmak, A.E. Salvucci, L.D. Geohring, A.G. Hay, J.-Y. Parlange, T.S. Steenhuis, Environ. Sci. Technol. 44 (13) (2010) 4965–4972.
[24] Y. Zevi, A. Dathe, J.F. McCarthy, B.K. Richards, T.S. Steenhuis, Environ. Sci. Technol. 39 (18) (2005) 7055–7064.
[25] S. Veerapaneni, J.M. Wan, T.K. Tokunaga, Environ. Sci. Technol. 34 (12) (2000) 2465–2471.
[26] B. Gao, T.S. Steenhuis, Y. Zevi, V.L. Morales, J.L. Nieber, B.K. Richards, J.F. McCarthy, J.-Y. Parlange, Water Resour. Res. 44 (2008) W04504, http://dx.doi.org/10.1029/2006WR005332.
[27] B. Gao, J.E. Saiers, J. Ryan, Water Resour. Res. 42 (1) (2006) W01410. http://dx.doi.org/10.1029/ 2005WR004233.
[28] S.A. Bradford, S. Torkzaban, Vadose Zone J. 7 (2) (2008) 667–681.
[29] P.A. Kralchevsky, K. Nagayama, Adv. Colloid Interf. Sci. 85 (2000) 145–192, http://dx.doi.org/10.1016/S0001-8686 (99)00016-0.
[30] S. Sirivithayapakorn, A. Keller, Water Resour. Res. 39 (12) (2003) 1346, http://dx.doi.org/10.1029/2003WR002487.
[31] J.T. Crist, Y. Zevi, J.F. McCarthy, J.A. Throop, T.S. Steenhuis, Vadose Zone J. 4 (2005) 184–195.
[32] M.H. Adams, Bacteriophages, Interscience, New York, N.Y., 1959. pp. 450–454.
[33] V.I. Syngouna, C.V. Chrysikopoulos, Environ. Sci. Technol. 44 (2010) 4539–4544, http://dx.doi.org/10.1021/es100107a.
[34] X. Rong, Q. Huanga, X. He, H. Chen, P. Cai, W. Liang, Colloids Surf. B: Biointerf. 64 (2008) 49–55.
[35] C.V. Chrysikopoulos, V.I. Syngouna, Colloids Surf. B: Biointerf. 92 (2012) 74–83.
[36] A. Graciaa, G. Morel, P. Saulner, J. Lachaise, R.S. Schechter, J. Colloid Interf. Sci. 172 (1995) 131–136.
[37] P.N. Mitropoulou, V.I. Syngouna, C.V. Chrysikopoulos, Chem. Eng. J. 232 (2013) 237–248, http://dx.doi.org/10.1016/j.cej.2013.07.093.
[38] C.V. Chrysikopoulos, V.I. Syngouna, Environ. Sci. Technol. 48 (2014) 6805–6813, http://dx.doi.org/10.1021/es501295n.
[39] S.C. James, C.V. Chrysikopoulos, Adv. Water Resour. 34 (2011) 1249–1255, http://dx.doi.org/10.1016/j.advwatres.2011.06.001.
[40] K.M. Yao, M.T. Habibian, C.R. O'Melia, Environ. Sci. Technol. 5 (11) (1971) 1105–1112.
[41] J.E. Saiers, J.J. Lenhart, Water Resour. Res. 39 (1) (2003) 1019, http://dx.doi.org/10.1029/2002WR001370.
[42] N. Tufenkji, M. Elimelech, Environ. Sci. Technol. 38 (2004) 529–536.
[43] J.P Murray, G.A Parks, in: M.C. Kavanaugh, J.O. Leckie (Eds.), Particulates in Water: Characterization, Fate, Effects and Removal, Adv. Chem. Ser., vol. 189, American Chemical Society, Washington, DC, 1978.
[44] H. Feng, Z. Yu, P.K. Chu, Mat. Sci. Eng. Rep. 54 (2006) 49–120.
[45] H. Van Olphen, J.J Fripiat, Data Handbook for Clay Minerals and Other Non-metallic Minerals, Pergamon Press, Oxford, England, 1979, p. 346.
[46] J.N. Israelachvili, Intermolecular and Surface Forces, 2nd ed., Academic Press, London, 1992.
[47] B.E. Novich, T.A. Ring, Clays Clay Miner. 32 (5) (1984) 400–406.
[48] B. Michen, F. Meder, A. Rust, J. Fritsch, C. Aneziris, T. Graule, Environ. Sci. Technol. 46 (2012) 1170–1177.
[49] J. Visser, Adv. Colloid Interf. Sci. 15 (2) (1981) 157–169.
[50] C.J. van Oss, J. Visser, D.R. Absolom, S.N. Omenyf, A.W. Neuman, Adv. Colloid Interf. Sci. 18 (3-4) (1983) 133–148.
[51] A.W. Neumann, J. Visser, R.P. Smith, S.N. Omenyf, D.W. Francis, E.B. Vargha-Butlerl, W. Zingg, C.J. van Oss, D.R. Absolom, Powder Technol. 37 (1) (1984) 229–244.
[52] P.A. Kralchevsky, J. Colloid Interf. Sci. 137 (1990) 217–233, http://dx.doi.org/10.1016/0021-9797 (90)90058-V.
[53] P.A. Kralchevsky, N.D. Denkov, K.D. Danov, Langmuir 17 (2001) 7694–7705, http://dx.doi.org/10.1021/la0109359.
[54] P.A. Kralchevsky, I.B. Ivanov, K.P. Ananthapadmanabhan, A. Lips, Langmuir 21 (2005) 50–63, http://dx.doi.org/10.1021/la047793d.
[55] R. Attinti, J. Wei, K. Kniel, J.T. Sims, Y. Jin, Environ. Sci. Technol. 44 (2010) 2426–2432.
[56] W. Wu, Clays Clay Miner. 49 (5) (2001) 446–452.
[57] S. Torkzaban, S.M. Hassanizadeh, J.F. Schijven, H.H.J.L. van den Berg, Water Resour. Res. 42 (2006) W12S14, http://dx.doi.org/10.1029/2006WR004904.
[58] P.A. Shields, S.R. Farrah, Determination of the electrostatic and hydrophobic character of enteroviruses and bacteriophages. Abstract Q-82, Program Abstracts of the 87th Annual Meeting of American Society of Microbiology, Washington, DC, 1987.
[59] V.I. Syngouna, C.V. Chrysikopoulos, J. Contam. Hydrol. 129–130 (2012) 11–24, http://dx.doi.org/10.1016/j.jconhyd.2012.01.010.
[60] Y. Jin, Y. Chu, Y. Li, J. Contam. Hydrol. 43 (2000) 111–128.
[61] J. Shang, M. Flury, Y. Deng, Water Resour. Res. 45 (2009) W06420, http://dx.doi.org/10.1029/2008WR007384.
[62] P. Sharma, M. Flury, J. Zhou, J. Colloid Interf. Sci. 326 (2008) 143–150.
[63] T. Knappenberger, M. Flury, E.D. Mattson, J.B. Harsh, Environ. Sci. Technol. 48 (2014) 3791–3799.
[64] Y. Sim, C.V. Chrysikopoulos, Water Resour. Res. 31 (5) (1995) 1429–1437, http://dx.doi.org/10.1029/95WR00199. Correction, Water Resour. Res. 32(5) (1996) 1473, doi:10.1029/96WR00675.
[65] C.J. Hurst, C.P. Gerba, I. Cech, Appl. Environ. Microb. 40 (1980) 1067–1079.
[66] C.P. Gerba, Adv. Appl. Microb. 30 (1984) 133–168.
[67] M.V. Yates, S.R. Yates, Crit. Rev. Environ. Control 17 (4) (1988) 307–344.
[68] C.V. Chrysikopoulos, A.F. Aravantinou, J. Hazard. Mater. 233–234 (2012) 148–157, http://dx.doi.org/10.1016/j.jhazmat.2012.07.002.
[69] S.S. Thompson, M. Flury, M.V. Yates, W.A. Jury, Appl. Environ. Microb. 64 (1998) 304–309.
[70] S.S. Thompson, M.V. Yates, Appl. Environ. Microb. 65 (1999) 1186–1190.